Supplementary materials

1. Knowledge-guided secondary screening

In each KI-DC-BO iteration, q-NEHVI generated a pool of ten candidate formulations within the current dynamically constrained feasible domain, as described in the main text. A knowledge-guided secondary screening step was then used to select 4 experimentally actionable formulations for resin preparation, 3D printing and property testing. This step operated only within the q-NEHVI-generated candidate pool. It did not replace the Gaussian-process surrogate models, did not directly predict material properties and did not generate new formulations.

The purpose of this screening step was to incorporate formulation knowledge and experimental actionability considerations that were difficult to fully encode in the acquisition function. For each candidate, the screening information included the formulation vector $(X_1, \ldots, X_6)$, the predicted objective values and uncertainties, the acquisition value and the active hard composition constraints. The selected candidates were required to satisfy the current dynamic constraints and the mass-balance requirement. Candidates predicted to approach the target region of $Y_1 \geq 90\,\mathrm{MPa}$, $Y_2 \geq 2.0\%$ and $Y_3 \geq 210^{\circ}\mathrm{C}$ were prioritized. Candidates with excessive IBOA, excessive total multifunctional-monomer loading or insufficient THEICTA were deprioritized because these regions were

associated with reduced mechanical or thermal balance and increased printing risk.

Candidate diversity was also considered to avoid selecting near-duplicate formulations in the same iteration. When chemically reasonable and within the active feasible domain, candidates with moderate predictive uncertainty could be retained to preserve exploration. The screening step therefore selected experimentally actionable formulations from the q-NEHVI candidate pool without changing the dynamic constraint boundaries. The experimental results of the selected formulations were then added to the accumulated dataset and used for the stage-level constraint refinement described in Section 3.

Supplementary Table S1 | Knowledge-guided secondary screening criteria for q-NEHVI candidates

Criterion	Purpose	Implementation in this work
Hard-constraint satisfaction	Keep selected candidates inside the active feasible domain	Selected candidates had to satisfy the current dynamic constraints and $\Sigma X_i = 100$
Predicted target-region performance	Prioritize balanced multi-objective candidates	Candidates predicted to approach ($Y_1 \geqslant 90$ MPa, $Y_2 \geqslant 2\%$ and $Y_3 \geqslant 210$ ℃) were prioritized
Monomer-blending priors	Incorporate experimentally derived formulation knowledge	Excessive (X_1), excessive ($X_3 + X_4 + X_5$) and insufficient (X_6) were deprioritized
Printing feasibility	Avoid high-risk experimental candidates	Candidates associated with poor resin handling, warping risk or failed printing regions were deprioritized
Candidate diversity	Avoid redundant experiments	Near-duplicate compositions were not selected together in the same iteration
Exploration under uncertainty	Preserve useful exploration	Chemically reasonable candidates with moderate predictive uncertainty could be retained

2. Regret-derived diagnostic metrics

Dynamic feasible-domain updating in KI-DC-BO was supported by empirical average-regret diagnosis and composition–property evidence. The regret analysis was used as a progress diagnostic to indicate when the current feasible domain should be reconsidered. The refined constraints were assigned by combining the regret diagnosis with experimentally observed composition–property evidence, including feature samples, boundary cases and monomer-blending priors.

Because the true global optimum in the experimental formulation space was unknown, theoretical regret could not be directly calculated. We therefore used a regret coefficient based on the current best experimentally observed performance. For each objective k, the objective-specific regret coefficient at iteration $t$was defined as

$$\beta_k(t) = \frac{Y_{k,\max}(t) - \bar{Y}_k(t)}{Y_{k,\max}(t) - Y_{k,\min}(t) + \varepsilon}$$

where $k = 1,2,3$ corresponds to tensile strength, elongation at break and T_g, respectively. $Y_{k,\max}(t)$ is the maximum value of objective $k$observed in all accumulated experimental data up to iteration t, $Y_{k,\min}(t)$ is the corresponding minimum or penalty-based low-performance reference value, $\bar{Y}_k(t)$ is the average measured value of the tested formulations in iteration t, and ε is a small constant used to avoid division by zero. A lower $\beta_k(t)$ indicates that the tested formulations in the current iteration

are closer to the current experimentally observed optimum for objective k.

The average regret over the three objectives was calculated as

$$\beta(t) = \frac{1}{3}\sum_{k=1}^{3} \beta_k\,(t)$$

The relative changing rate of the average regret was calculated as

$$R(t) = \frac{\beta(t) - \beta(t-1)}{\beta(t-1) + \varepsilon} \times 100\%$$

A constraint update was considered when $\beta(t)$, $\beta_k(t)$ or $R(t)$ showed stagnation, sharp variation or imbalance among the objectives, indicating that the current feasible domain was no longer providing balanced multi-objective improvement. The numerical constraint boundaries were then supported by experimentally observed composition–property evidence from feature samples and boundary cases, using interpretable descriptors including X_1, X_2, $X_3 + X_4 + X_5$ and X_6.

3. Stage-level constraint refinement

Dynamic constraint refinement in KI-DC-BO was performed at the optimization-stage level rather than after each individual experiment. The regret-derived diagnostics described above were first used to assess whether the current feasible domain continued to provide effective multi-objective improvement. When feasible-domain refinement was considered, the newly tested formulations were examined together with the empirical Pareto distribution, monomer-blending priors and composition–property

trends.

Constraint refinement was restricted to four interpretable composition descriptors: X_1, X_2, $X_3 + X_4 + X_5$ and X_6, corresponding to the IBOA fraction, ACMO fraction, total multifunctional-monomer fraction and THEICTA fraction, respectively. A candidate update was introduced only when high-value tested formulations showed a consistent trend in one or more of these descriptors and when this trend was consistent with the monomer-blending results. The revised constraint was accepted only if previously identified high-value formulations remained within the feasible domain and the updated domain still allowed sufficient candidate generation for the next q-NEHVI step.

4. Accepted constraint updates

The feature samples used to define the initial feasible domain and to support the two constraint updates are listed in Supplementary Tables S2–S4. In this work, feature samples refer to representative experimentally tested formulations that revealed composition–property characteristics relevant to feasible-domain refinement. These samples include formulations with balanced multi-objective performance as well as boundary samples that indicated unfavourable composition regions.

The accepted constraint updates during the KI-DC-BO campaign are summarized here. The initial feasible domain was defined using the

monomer-blending trends and the 30 initial experimental formulations. The starting constraints were:

$$X_1 \leq 10, X_2 \geq 10, X_3 + X_4 + X_5 \leq 20, X_6 \geq 50$$

The feature samples used to define this initial space are listed in Supplementary Table S1.

After the first optimization stage, Update I increased the ACMO lower bound from $X_2 \geq 10$ to $X_2 \geq 20$. The corresponding feature samples are listed in Supplementary Table S2. After the second optimization stage, Update II further refined the feasible domain by increasing the ACMO lower bound and tightening the total multifunctional-monomer constraint:

$$X_2 \geq 30, X_3 + X_4 + X_5 \leq 10$$

The corresponding feature samples are listed in Supplementary Table S3.Together, these feature samples record the experimental basis for the stage-level feasible-domain refinements used in KI-DC-BO.

Tab.S2 Feature samples of initial space

No.	X_1	X_2	X_3	X_4	X_5	X_6	Y_1	Y_2	Y_3
KBO-3	20	0	0	0	0	80	73	2.8	200
KBO-7	10	0	20	0	0	70	68	2	198
KBO-19	0	30	0	20	0	50	78	1.8	215
KBO-22	0	10	0	0	30	60	60	1.5	180
KBO-23	10	0	0	0	30	60	60	1.5	180
KBO-24	0	16.7	33.3	0	0	50	76	2	221

Tab.S3 Feature samples of Update I

No.	X_1	X_2	X_3	X_4	X_5	X_6	Y_1	Y_2	Y_3
KBO-37	1.7	19.9	0.9	2.5	4.2	70.8	85	2.0	231
KBO-43	1.7	17.8	1.3	0.1	3.8	75.3	79	1.7	235
KBO-45	0.0	20.0	0.0	0.0	7.2	72.8	86	2.2	230
KBO-46	0.1	25.8	0.1	0.1	3.8	70.1	93	2.1	228
KBO-8	0.0	10.0	0.0	0.0	0.0	90.0	86	1.5	231
KBO-9	0.0	20.0	0.0	0.0	0.0	80.0	89	2.1	226

Tab.S4 Feature samples of Update II

No.	X_1	X_2	X_3	X_4	X_5	X_6	Y_1	Y_2	Y_3
KBO-53	5.5	27.7	11.3	1.1	4.4	50.0	87	2.6	215
KBO-60	10.0	20.0	0.0	0.0	0.0	70.0	85	2	211
KBO-62	0	30	0	0	10	60	90	2	227
KBO-68	0.1	35.1	1.8	0.5	0.3	62.2	98	2.1	225
KBO-70	0.8	31.2	1.1	0.6	9.5	56.8	82	1.9	224
KBO-49	0.8	16.7	0.0	1.1	5.1	75.3	74	1.6	236

5. The pareto front samples

Table S5 Formulation and performance data of representative Pareto-front photopolymers after optimization

KBO	X_1	X_2	X_3	X_4	X_5	X_6	Y_1	Y_2	Y_3
33	0.0	20.3	0.0	0.0	4.4	75.3	88	1.9	230
36	0.4	14.6	2.6	2.6	9.8	70.1	82	1.9	234
43	1.7	17.8	1.3	0.1	3.8	75.4	79	1.7	235
45	0.0	20.0	0.0	0.0	7.2	72.8	86	2.2	230
46	0.1	25.8	0.1	0.1	3.8	70.0	93	2.1	227
51	0.2	34.8	0.1	2.5	3.5	58.9	96	2.5	218
58	1.0	37.0	1.5	0.0	1.5	59.0	99	2.4	217
68	0.1	35.1	1.9	0.4	0.3	62.2	98	2.1	225
71	1.8	34.8	0.1	1.2	0.6	61.5	95	2.3	224
80	2.2	36.2	1.5	0.2	1.8	58.1	103	2.7	213
82	0.1	36.5	0.2	1.4	2.4	59.4	101	2.8	214
85	1.0	37.0	0.0	1.5	2.5	58.0	98	2.1	220

6. Regret analysis of the optimization

The convergence of KI-DC-BO was evaluated using the objective-specific regret coefficients, the average regret $\bar{\beta}$ and the relative change of $\bar{\beta}$. Supplementary Fig. S1a shows the evolution of the regret coefficients for tensile strength, T_g and elongation at break during the 15 optimization iterations. Supplementary Fig. S1b shows the corresponding average regret $\bar{\beta}$ and its relative change. The regret-derived metrics fluctuated during the early and middle stages, reflecting active feasible-domain refinement and multi-objective exploration. In the later iterations, both $\bar{\beta}$ and its relative change became more stable, supporting the

convergence assessment by the 15th iteration. This regret-based convergence behaviour is consistent with the hypervolume stabilization shown in Fig. 4e.

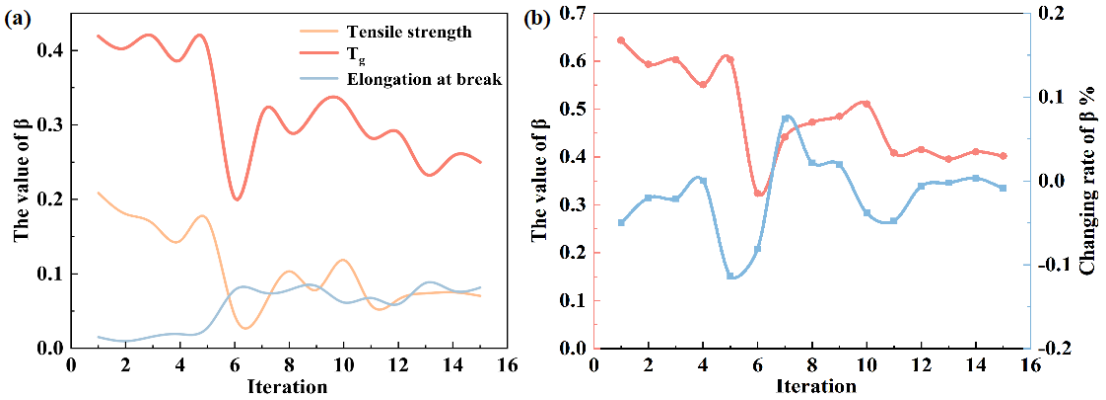

Supplementary Fig. S1 | Regret-derived convergence diagnostics during KI-DC-BO. a, Evolution of the objective-specific regret coefficients for tensile strength, glass-transition temperature T_g and elongation at break over 15 optimization iterations. **b**, Evolution of the average regret $\bar{\beta}$ and the relative change of $\bar{\beta}$. The stabilization of the regret-derived metrics in the later iterations supports the convergence assessment of the KI-DC-BO process.

7. Benchmark data for tensile strength–T_g comparison

Supplementary Table S6 | Benchmark data and testing conditions used for Fig. 5b

Manufacturer	Grade/ Category	Tensile strength MPa	T_g °C
LOCTITE[1]	3D IND147	67±16	205-212
Nexa 3D[2]	xPRO9400-FR	78	175
Stratasys[3]	P3 Deflect 110	75	143
Liqcreate[4]	Strong-X	60-84	128
Carbon[5]	EPX 86FR	90-94	150
Forward AM[6]	Ultracur3D RG 1100	70	131
Benzoxazine[7]	IPNs	92	188
Diisocyanate[8]	IPNs	85	210
hBN-KH560[9]	IPNs	73	150
This work	KBO-33	88	230
	KBO-68	98	225
	KBO-80	103	213

1 https://formlabs-media.formlabs.com/datasheets/2301761-TDS-ENUS-0.pdf
2 https://dm.henkel-dam.com/is/content/henkel/Loctite-3D-IND147
3. https://nexa3d.com/wp-content/uploads/2023/11/Nexa3D_xPRO9400-FR_TDS.pdf

4. https://www.stratasys.com/en/materials/materials-catalog/p3-materials
5.https://www.liqcreate.com/downloads/tds/TDS%20Liqcreate%20StrongX%20V4%20June2021.pdf
6. https://docs.carbon3d.com/files/technical-data-sheets/tds_carbon_epx-86fr.pdf
7. https://doi.org/10.1016/j.cej.2023.147221
8. https://doi.org/10.1002/mame.202000397
9. https://doi.org/10.1016/j.compscitech.2026.111635